

Active Sampling for MRI-based Sequential Decision Making

Yuning Du, Jingshuai Liu, Rohan Dharmakumar, and Sotirios A. Tsaftaris

Abstract— Despite the superior diagnostic capability of Magnetic Resonance Imaging (MRI), its use as a Point-of-Care (PoC) device remains limited by high cost and complexity. To enable such a future by reducing the magnetic field strength, one key approach will be to improve sampling strategies. Previous work has shown that it is possible to make diagnostic decisions directly from k -space with fewer samples. Such work shows that single diagnostic decisions can be made, but if we aspire to see MRI as a true PoC, multiple and sequential decisions are necessary while minimizing the number of samples acquired. We present a novel multi-objective reinforcement learning framework enabling comprehensive, sequential, diagnostic evaluation from undersampled k -space data. Our approach during inference actively adapts to sequential decisions to optimally sample. To achieve this, we introduce a training methodology that identifies the samples that contribute the best to each diagnostic objective using a step-wise weighting reward function. We evaluate our approach in two sequential knee pathology assessment tasks: ACL sprain detection and cartilage thickness loss assessment. Our framework achieves diagnostic performance competitive with various policy-based benchmarks on disease detection, severity quantification, and overall sequential diagnosis, while substantially saving k -space samples. Our approach paves the way for the future of MRI as a comprehensive and affordable PoC device. Our code is publicly available at https://github.com/vios-s/MRI-Sequential_Active_Sampling.

Index Terms— Computer aided diagnosis, Magnetic resonance imaging, Point of care, Reinforcement learning.

I. INTRODUCTION

DESPITE the proliferation of MRI, its utility as a Point Of-Care (PoC) diagnostic tool remains limited due to prolonged acquisition times, complex instrumentation, and high cost [1]. A promising solution has emerged through the development of low-field MRI systems [2]. These systems

Manuscript received May 9, 2025. This work was supported in part by National Institutes of Health (NIH) grant 7R01HL148788-03. Yuning Du thanks additional financial support from the School of Engineering, the University of Edinburgh. Sotirios A. Tsaftaris acknowledges support from the Royal Academy of Engineering and the Research Chairs and Senior Research Fellowships scheme (grant RCSR1819\8\25), and the UK Engineering and Physical Sciences Research Council (EPSRC) support via grant EP/X017680/1, and the UKRI AI programme, Causality in Healthcare AI Hub (CHAI, grant EP/Y028865/1).

Yuning Du, Jingshuai Liu and Sotirios A. Tsaftaris are with the School of Engineering, University of Edinburgh, Edinburgh EH16 4UX, U.K. (e-mail: yuning.du@ed.ac.uk; jliu11@ed.ac.uk; s.tsafaris@ed.ac.uk).

Rohan Dharmakumar is with the Cedars Sinai Medical Center, Los Angeles, CA 90048 USA (e-mail: rohan.dharmakumar@cshs.org).

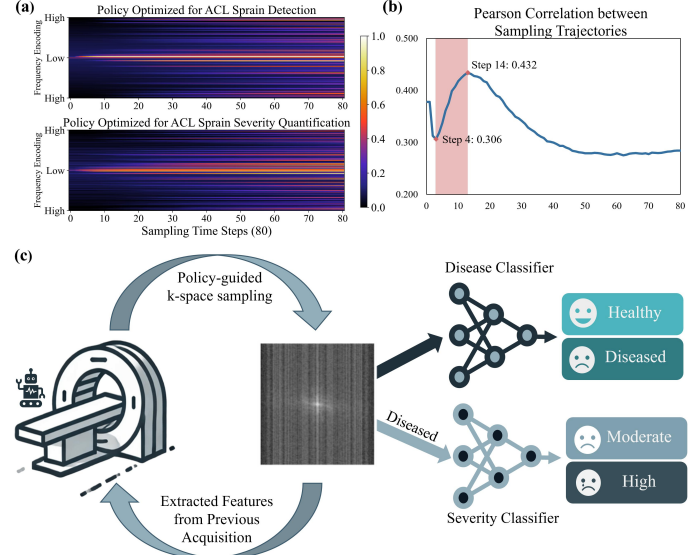


Fig. 1. Illustration of our proposed sequential diagnostic framework for active MR acquisition and its motivating evidence: in preliminary experiments, we found similarities between the sampling trajectories of disease detection and severity quantification. We trained policies [4] optimized independently for each task and obtained sampling trajectories shown in (a), and then measured their similarity in (b). We observe an increasing Pearson correlation between sampling steps 4 and 14, indicating that in this range k -space samples contribute simultaneously to both tasks. These observations motivate our approach (c) to learn a sampling policy that jointly optimizes two tasks, taking into account their sequential nature. During inference, our approach identifies which samples to take using k -space features, considering that one task (severity) will be following the confirmation of the disease.

can be deployed at accident sites, in ambulatory settings, or in other areas where immediate decisions are necessary to provide the best treatment options. Thus, such PoC settings are not to replace the utility of MRI as a clinical generic diagnostic tool, but as a bespoke affordable and portable device. However, a reduced magnetic field strength [3] does degrade imaging quality. Therefore, improvements in how and where we sample are considered key for unlocking the future of MRI as PoC.

Recent advances in machine learning methods have allowed a reduction in k -space samples and retaining diagnostic utility [5]. A line of work has focused on optimizing sampling trajectories for image reconstruction [6], [7]. More recently, exciting approaches have emerged that aim to drastically reduce sampling by removing redundant information. These methods bypass image reconstruction entirely and make direct

inferences from undersampled k -space [8], [9].

Decisions even in a PoC setting will be complex and reflect a multilayered decision making process. Hence, high-level decisions (e.g., disease presence) should be made first, followed by additional decisions (e.g., disease severity) to determine subsequent actions (e.g., treatment options). A fundamental research question emerges: *Are there correlations in k -space patterns between such sequential decisions and can these be exploited for further sampling reductions?* If such correlations exist, sampling strategies should be optimized to exploit them. Otherwise, independently optimizing sampling strategies for each diagnostic task leads to sampling inefficiency. Our preliminary experiments (Figure 1) reveal compelling correlation patterns between sampling trajectories.

Leveraging this observation, we develop an AI agent to satisfy both objectives within the same policy, maintaining computational efficiency while structuring binary diagnostics as a structured sequential decision process for comprehensive clinical assessment. To the best of our knowledge, such active sampling strategies for sequential diagnostic tasks have not been previously explored. We reformulate the diagnostic process as a multi-objective reinforcement learning (MORL) sampling optimization problem, sequentially inferring the presence of the disease and its severity in one scanning session.

As illustrated in Figure 1, the core components of our framework include: an RL-based policy network for k -space sampling guidance, and dual diagnostic streams for disease detection and severity quantification. The policy network guides data acquisition by leveraging features extracted from accumulated k -space measurements, continuously optimizing the sampling trajectory. The diagnostic streams process the undersampled k -space hierarchically: the disease classifier performs binary classification to identify diseased subjects, which is followed by severity quantification for positive cases.

Overall, our **contributions** are summarized as follows:

- Our research pioneers sequential, dynamic diagnosis from k -space data with active sampling, enabling sequential decisions in a single scanning session.
- A MORL-based policy network employs policy gradient methods with greedy action selection for efficient k -space exploration. It optimizes a step-wise weighting reward function to balance disease detection and severity quantification, maximizing diagnostic information gain.
- Extensive experiments on ACL sprain detection and cartilage thickness loss assessment demonstrate that our method outperforms baselines and benchmarks in diagnostic accuracy, and significantly reduces k -space data acquisition time, advancing PoC MRI applications.

II. RELATED WORKS

We first review ML-based k -space sampling optimization techniques that accelerate acquisition. We then examine direct diagnostic inference approaches from k -space, highlighting the research gap in sequential decision making. Finally, we discuss RL-based multi-objective optimization in medical imaging, demonstrating how our sequential sampling framework builds upon these foundations to enable comprehensive diagnosis directly from undersampled k -space.

A. ML-based k -space Sampling Optimization

Accelerating MRI acquisition remains a significant research focus through improved k -space undersampling strategies. While the Cartesian grid trajectory predominates in clinical practice due to its robustness [10], conventional undersampling approaches—including equispaced, random, and variable density sampling—prioritize frequency domain characteristics rather than task-specific requirements, potentially compromising clinical accuracy in accelerated acquisitions [11].

Recent works have advanced learning-based sampling methods that optimize diagnostic performance at the population level. These approaches formulate sampling mask optimization either as a probability density function for Cartesian grid selection [6], [12] or as learnable non-Cartesian coordinates [13] in non-uniform Fast Fourier Transform (NUFFT) [14], [15], enabling end-to-end optimization of sampling trajectories and reconstruction performance. While subsequent innovations incorporate generative models [16] and model pruning [17], these methods produce fixed sampling patterns that do not adapt to patient-specific characteristics.

Instead, active sampling strategies adapt to individual patients through sequential k -space measurements. Reinforcement learning (RL) has emerged as a powerful framework for this sampling optimization, framing k -space sampling as a Markov Decision Process where policies learn to select measurements based on accumulated information. Notable approaches include policy gradient methods with greedy actions [18] and Q-learning [19] for reconstruction optimization. While initial work focused on reconstruction quality, recent studies demonstrate the potential for direct diagnostic inference from undersampled data [20], indicating a paradigm shift from traditional reconstruction-based analysis to efficient, direct k -space diagnostic assessment.

B. Direct Diagnostic Inference from k -space

A new line of work has shown the potential of ‘imageless’ diagnostic processes through direct inference from k -space data. This approach reduces the need for reconstruction, saving samples by avoiding redundant and uninformative pixels (voxels). Studies show successful disease classification [4], [8], [9] and segmentation [20] using undersampled k -space measurements, without reconstruction. Direct inference with population-level undersampling optimization achieves comparable performance to fully-sampled image analysis, while integration with RL-based active sampling enables patient-level mask optimization and improved classification performance [4], [9]. However, existing approaches primarily optimize sampling for a single objective during a scanning session, leaving multi-objective sampling optimization unexplored. As such any additional redundancy between the sampling patterns for different tasks (and hence different objectives) is unutilized.

C. RL-based Multi-objective Optimization in Medical Imaging

Multi-objective optimization in clinical evaluation systems presents a fundamental challenge in medical imaging. While

multi-task learning frameworks have been explored extensively [21], [22], the joint optimization of sampling strategies for multiple diagnostic targets remains underexplored. Recent advances in MORL show promising methodological innovations across medical applications [23]. In chest X-ray generation [24], policy-based RL simultaneously optimizes posture alignment, diagnostic conditions, and multimodal consistency through cumulative reward maximization. Similarly, anatomical landmark detection [25] leverages multi-agent frameworks with specialized joint detection while preserving anatomical constraints. Further innovations include consequence-oriented reward functions for simultaneous vertebral detection and segmentation [26], incorporating exponentially weighted attention metrics for balanced task performance.

While various frameworks demonstrate efficacy through weighted rewards [26], [27] and collaborative strategies [25], [28], their application to k -space sampling optimization remains unexplored, presenting opportunities for frameworks that simultaneously optimize multiple diagnostic goals.

III. METHODOLOGY

A. Preliminaries

Instead of directly imaging human anatomy, MRI captures the electromagnetic activity in the body after exposure to magnetic fields and radio-frequency pulses, measured in k -space (i.e., the frequency domain). For a single coil measurement, the k -space data can be represented as a 2-dimensional complex-valued matrix $\mathbf{x} \in \mathbb{C}^{r \times c}$, where r is the number of rows and c is the number of columns, respectively. The spatial image \mathbf{I} is obtained by applying the inverse Fourier Transform to \mathbf{x} , denoted as $\mathbf{I} = \mathcal{F}^{-1}(\mathbf{x})$. The undersampled k -space, represented as \mathbf{x}_s , is modeled by $\mathbf{x}_s = U_L \circ \mathbf{x}$ where U_L can be viewed as a binary mask $U \in \{0, 1\}^{r \times c}$ with L measurements sampled in k -space. We exclusively consider a Cartesian mask for MRI undersampling. Thus, the undersampled image is denoted as $\mathbf{I}_s = \mathcal{F}^{-1}(\mathbf{x}_s)$.

For clinical diagnosis, radiologists and other clinical experts interpret medical imaging data to first identify the presence of disease (g_d) and then its severity (g_s), providing a comprehensive diagnosis. These labels are derived by analyzing the collected k -space data after appropriate processing.

B. Framework Workflow

As shown in Figure 2, our framework aims to reduce acquisition time by selectively and progressively sampling the k -space, considering sequential diagnostic tasks.

The process begins with a small subset of randomly sampled k -space with L measurements, denoted as $\mathbf{x}_{s_0} = U_L \circ \mathbf{x}$, which is passed to task-specific classifiers. The pre-trained disease and severity classification networks f_d and f_s , generate the initial disease and severity prediction y_{d_0} and y_{s_0} . The high-level feature maps m_0 , from both classifiers are extracted and then fed into the *Active Sampler* S , where the policy network, parameterized by ϕ , generates a sampling policy $\pi_\phi(m_0)$ to guide the selective sampling of diagnostically significant lines in k -space. These sampled lines are subsequently added to U_L . The updated k -space subset at step $t \in [0, T]$ is denoted

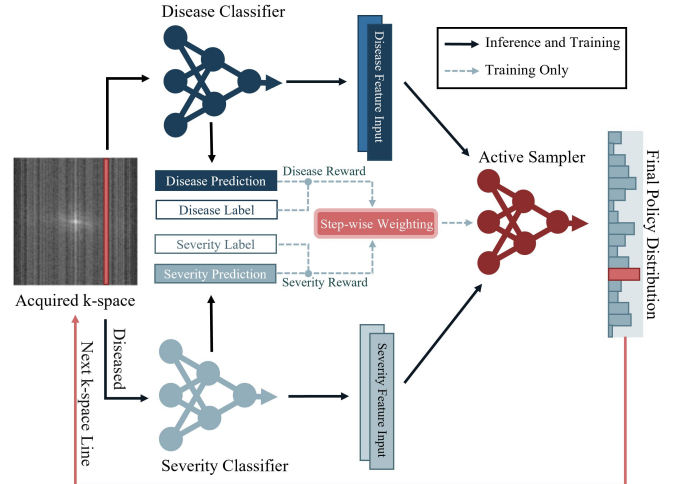


Fig. 2. Illustration of the proposed sequential diagnostic active sampling. Initially, a randomly sampled k -space subset is fed into two pre-trained disease and severity classifiers. The active sampler takes as input the features extracted by the classifiers and decides the next k -space sampling location. After exhausting the sampling budget or meeting a user-defined criterion, the disease classifier confirms the presence of disease and subsequently the severity classifier is queried to estimate the severity level. During training, the active sampler is optimized with a novel step-wise weighting mechanism that combines the disease and severity rewards and enables a smooth transition.

as $\mathbf{x}_{s_t} = U_t \circ \mathbf{x}$ and fed back into the classification network. The iterative process continues until the sampling budget T is exhausted or some user-defined reliability criterion (e.g., confidence score) is satisfied. During the training stage, we separately calculate the disease reward $r_d = r(y_d, g_d)$ and severity reward $r_s = r(y_s, g_s)$ using classifier predictions and the ground truth labels. An obvious and naive approach would be to directly use the rewards to supervise the active sampler; however, this will not learn the sequential aspect of the two objectives. Instead, we propose here to use a step-wise weighting procedure to shift the emphasis of sampling strategy from one objective to the other as sampling steps progress. In addition, to further enforce the sequential nature (i.e., disease prediction should precede severity), if the disease prediction is ‘No findings’ for a subject, the severity reward will not be applied for supervision.

C. Undersampled k -Space Classification Networks

To perform direct prediction with undersampled k -space data, we pre-train a disease classifier f_d with undersampled data and ground truth label g_d . For the severity classifier f_s , we fine-tune the disease classifier with only diseased data and the associated severity labels g_s . For severity quantification, fine-tuning prevents potential overfitting caused by data scarcity and reuses the knowledge learned by the disease classifier. These pre-trained classifiers act as the reward model in the training process of the active sampler. They also function as a feature extractor, providing complex and informative feature maps m_t per sampling step as part of the internal state.

D. Multi-objective k -Space Active Sampler

1) *Problem Formulation*: Building on prior works in RL-based k -space active sampling strategies [4], [18], [19], the sequential selection of k -space is formalized as a Partially Observable Markov Decision Process (POMDP) [29].

The latent state z_t at acquisition step t is defined as $z_t = (\mathbf{x}, g_d, g_s, h_t)$, where \mathbf{x} represents the underlying MRI k -space, g_d and g_s denote the disease condition and severity levels, and h_t encapsulates the history of actions and observations up to time t as $h_t = (a_0, o_0, \dots, a_{t-1}, o_{t-1})$. Each action a_t corresponds to the selection of a specific k -space line for measurement, while o_t represents the corresponding measurement obtained from that location. The inclusion of \mathbf{x} in the latent state represents the ground truth data from which k -space measurements are derived, fundamentally linking the observation model to the true anatomical structure. The agent maintains an internal state composed of high-level features m_t that combine disease and severity features from the corresponding classifiers, and predictions y_t including disease prediction y_{dt} and severity prediction y_{st} , which summarize the history h_t . The agent outputs a policy $\pi(a_t|m_t)$ over possible k -space line selections with only high-level feature representation as input. The reward function $r(z_t, a_t)$ reflects improvements in both disease classification and severity quantification accuracy, weighting their respective contributions through a step-wise mechanism, as discussed below.

2) *Policy Gradient-based Sampler with Greedy Action*: In our framework, the POMDP problem is solved via Policy Gradient with greedy action. Specifically, we maximize the expected return $J(\phi)$ of a policy π_ϕ parameterized by ϕ . At each step, the overall classification improvement is calculated as $r(y_{t+1}, y_t) = \eta(y_t, g) - \eta(y_{t+1}, g)$, where r represents the reward computed with criterion η (cross entropy) between predictions y and ground truth labels $g = (g_d, g_s)$.

During training, we accelerate the learning process by sampling q lines with the highest policy probabilities in parallel. The greedy selection method facilitates efficient action space exploration. Technically, we average their accumulated action rewards as feedback for model optimization [30] and randomly select one of the q samples as the executed action of the policy. As no greedy action is applied during inference, the trained policy samples one line at each step. We sample q lines at each step to calculate the following estimator:

$$\nabla_\phi J(\phi) \approx \frac{1}{q-1} \mathbb{E}_{\mathbf{x}} \left[\sum_{i=1}^q \sum_{t=L}^{T-1} \right. \\ \left. [\nabla_\phi \log \pi_\phi(m_t)] (r_{i,t} - \frac{1}{q} \sum_{j=1}^q r_{j,t}) \right], \quad (1)$$

where $r_{i,t}$ is the reward of sample i at step t . This equation estimates the gradient $\nabla_\phi J(\phi)$ to update the policy π_ϕ .

3) Step-wise Reward Weighting with Lexicographic Ordering

As mentioned in Sec. II-C, a crucial challenge in multi-objective k -space sampling is to jointly optimize multiple objectives without compromising performance. One naive solution is to respectively compute the rewards for the two tasks (here disease detection and severity quantification) and use

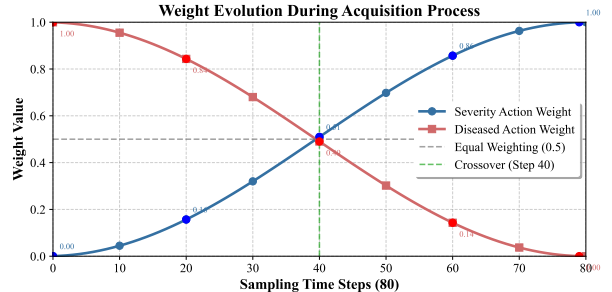


Fig. 3. Step-wise weighting evolution for multi-objective diagnosis following lexicographic ordering. The step-wise weight dynamically determines the preference of the reward feedback in disease detection and severity quantification objectives, which ensures a smooth transition.

the total reward as feedback for policy update. However, this ignores the natural order of these two tasks: one first detects disease presence and only if disease is present, the degree of severity is quantified, which aligns with the standard interpretation workflow of radiologists [31]. Following such diagnostic order, we expect the sampling framework to primarily promote disease detection performance in the early stage and focus on severity quantification in the later stage. Consequently, to accomplish these tasks with MORL, we formulate the process as a lexicographic ordering problem [32], where the order of the two objectives is fixed and the weight is dynamically adjusted by *cosine interpolation* [33] during the sampling process to ensure a smooth transition. Thus, the weighted sum reward with cosine interpolation is defined in Eq. 2a, with step-wise weights calculated via Eq. 2b and Eq. 2c:

$$r(t) = w_{disease}(t) * r_d(t) + w_{severity}(t) * r_s(t) \quad (2a)$$

$$w_{severity}(t) = \frac{1}{2} (1 - \cos(\pi \cdot \frac{t+1}{T} + \pi\beta)) \quad (2b)$$

$$w_{disease}(t) = 1 - w_{severity}(t), \quad (2c)$$

where r_d and r_s denote disease detection and severity quantification rewards, t is the current step, T is the total acquisition steps, and β denotes a weight parameter which adjusts the equal weighting point. Here we set β to be 0. The transition of the two objectives is also illustrated in Figure 3. It is shown that by step-wise weighting, the reward function emphasizes the feedback of the disease detection task in the early stage and smoothly transitions to the quantification of severity.

IV. EXPERIMENTAL SETUP

A. Dataset and Pre-processing

Dataset: Experiments are conducted with the single-coil k -space data and slice-level labels from the publicly available fastMRI dataset [34] and fastMRI+ dataset [35]. We use 1,172 annotated volumes from the fastMRI Knee dataset to validate the performance of our framework in two types of pathology diagnosis and severity quantification: *ACL Sprain (High Grade/Low-Moderate Grade)* and *Cartilage Thickness Loss (Full/Partial)*. We follow the data split provided by the dataset, resulting in the distribution of Table II.

Data Pre-processing: Since the k -space data have varying sizes, we first apply inverse Fourier transform to obtain the

TABLE I

OBJECTIVES, DIAGNOSTIC SUPPORT, AND INFERENCE DATA OF IMPLEMENTED METHODS. THE OBJECTIVE OF POLICY RECON IS IMAGE RECONSTRUCTION

Method	Diagnostic Objectives			Diagnostic Strengths		Data Used for Inference	
	Disease Detection	Severity Quantification	Overall Diagnosis	Sampling Optimization	Sequential Diagnosis	Undersampled k -space	Full k -space
<i>Fully Sampled</i>	○	○	○				✓
<i>Undersampled</i>	○	○				✓	
<i>Policy Recon</i> [18]	-	-	-	✓		✓	
<i>Policy Classifier</i> [4]	○	○		✓		✓	
<i>Simulated Policy</i>			○	✓		✓	
<i>Varying Parameter Policy</i>	●	●	●	✓		✓	
Weighted Policy (Ours)	●	●	●	✓	✓	✓	✓

○ : Objective optimized independently (one objective per strategy) ● : Multiple objectives optimized simultaneously within a single strategy

TABLE II

TRAIN-VAL-TEST SPLIT FOR ACL SPRAIN AND CARTILAGE THICKNESS LOSS DATASETS

Pathology	ACL Sprain			Cartilage Thickness Loss		
	No Finding	Low-Mod Grade	High Grade	No Finding	Partial	Full
Severity Degree						
Train	30915	617	503	29768	1850	417
Validation	5180	56	58	4907	325	62
Test	1734	42	65	1732	79	30
Total	37829	715	626	36407	2254	509

fully sampled k -space data to get the ground truth image and crop it to size (320×320) for computational efficiency. After applying Fourier transform to the ground truth image, we obtain the ground truth k -space data. There is a severe class imbalance between the two diagnostic tasks. To address it during training, we use weighted cross-entropy loss based on the label distribution to avoid overfitting to the majority class and poor generalization on the minority class. When training the policy network, we undersample the data for computational savings, as suggested in [4], [18].

B. Baselines and Benchmarks

We design benchmark methods and baselines based on different diagnostic strengths, data access, and objectives as shown in Table I, to fairly evaluate our approach.

1) *Fully Sampled Classifier (Oracle)*: This serves as an oracle benchmark for classifier performance with fully sampled k -space data as input, and hence no sampling optimization occurs. We trained the disease classifier with the ground truth images which are derived from fully sampled k -space data and supervised by the disease level label. The severity classifier is fine-tuned from the well-trained disease classifier with only diseased subjects and their severity label. The sequential diagnosis results are inferred by connecting disease and severity classifiers together. We refer to it as *Fully Sampled*.

2) *Undersampled Classifier*: The classifier serves as a baseline for single binary tasks, such as disease diagnosis and severity quantification, with the inverse Fourier transform applied to the randomly undersampled k -space data and no sampling optimization. It adopts the same backbone as the *Oracle* and is trained with undersampled images with various sample rates (5% to 30%) and center fraction (0% to 5%), supervised as before. We refer to it as *Undersampled*.

3) *Single-task Oriented Methods*: The methods introduced here are designed for single-task evaluation, targeting binary diagnosis of disease detection or severity quantification.

Policy Classifier [4]: This diagnosis-oriented policy benchmark optimizes patient-level sampling in k -space for direct

inference, setting the upper bound for disease detection and severity quantification. For disease detection, we use a backbone similar to *Undersampled* as a pre-trained classifier. For severity quantification, the classifier is fine-tuned from the disease detection model. Sampling policy rewards are computed via weighted cross-entropy predictions, with feature maps from the pre-trained classifier as input to the policy network. Training starts with a 5% initial sample rate, progressively sampling 80 lines to reach a 30% budget.

Policy (via) Reconstruction [18]: This model optimizes patient-level sampling with image reconstruction error as rewards, providing a comparison when reconstruction is involved in diagnosis. We pre-train a U-Net [36] with a 16-channel first feature map and 4 pooling cascades, totaling 837K parameters. The model is trained across sampling rates (5%–30%) with a 5% center fraction, supervised using ℓ_1 loss. The active sampler, built on the reconstruction model, uses reconstructed images as input and optimizes sampling with SSIM [37] as the reward. This cascaded design totals 26.7M parameters. Its diagnostic evaluation adopts the *Oracle* classifiers, which are trained to make predictions from fully sampled images, leading to the Policy-based Reconstruction Network (*Policy Recon*).

4) *Multi-task oriented Methods for Comprehensive Diagnosis*: These diagnosis-oriented methods are designed for multi-task evaluation, aiming to provide a comprehensive diagnosis of the presence and severity of disease. These methods do not consider the order of objectives and enforce sequential steps.

Simulated Policy Classifier: This benchmark evaluates a single-objective reinforcement learning (RL) policy network tailored for comprehensive diagnosis. It adopts a similar architecture to our framework, e.g., extracting the high-level features from the pre-trained disease and severity classifiers, while using a different rewarding mechanism. Instead of relying on step-wise weighting to adjust the diagnostic rewards, this policy is optimized via a reward function that unifies the diagnostic outcomes as the F1-score of a three-class classification task, where the final diagnosis is categorized as: (0) no findings, (1) diseased with low severity, and (2) diseased with high severity. This formulation simulates the situation where the model simultaneously infers both the presence and severity of disease, without enforcing sequential steps. We refer to this approach as *Simulated Policy*.

Varying Parameter Policy Classifier: To benchmark diagnosis using multi-objective reinforcement learning (MORL) without specifying the optimization order of objectives, we

introduce a method based on the varying parameter approach [38]. This method employs two separate policy networks—one for disease detection and another for severity quantification—designing sampling trajectories independently before averaging their outputs to guide k -space selection. Each policy is trained with its individual reward, but during joint training, the severity policy considers rewards only from diseased subjects, ignoring others. This approach is termed *Varying Parameter Policy*.

5) Weighted Sequential Policy Classifier (Ours): Our proposed method, introduced in Section III is a MORL-based policy network coupled with a step-wise weighting mechanism. The pre-trained disease classifier shares the same backbone as *Undersampled* and only has access to undersampled k -space data. The severity classifier is fine-tuned from the well-trained disease classifier. Both classifiers are utilized to provide step-wise weighting rewards and high-level feature representations to the policy network as illustrated in Figure 2. During joint training, only when the input subject is diseased does the severity reward from the classifier get used. Our method is referred to as *Weighted Policy*.

C. Evaluation Metrics

To assess diagnostic performance, we evaluate our method from three perspectives: disease detection, severity quantification, and overall sequential diagnosis, using Area Under the Receiver Operating Characteristic curve and Balanced Accuracy as primary metrics. For disease detection, we assess the model’s ability to distinguish pathological cases from no findings. Severity quantification focuses on positive cases, evaluating accuracy in classifying disease progression (Low-Moderate vs. High Grade for ACL Sprain; Partial vs. Full for Cartilage Thickness Loss). Sequential diagnosis treats the process as trajectory prediction, requiring correct classification at both stages—detecting disease and assessing severity—for a prediction to be valid, aligning with real-world clinical needs.

D. Implementation Details

All classification networks employed share the same ResNet-50 [39] backbone with 25.6M parameters. To avoid overfitting caused by class imbalance, a dropout layer is added at the end, and weighted cross-entropy is used as the supervised learning loss [40]. For methods involving a policy with greedy actions, we use the policy gradient network (11M parameters) [4], [18] with parallel acquisition $q = 8$. For all methods, we employ the Adam optimizer [41] with a learning rate of 10^{-4} and a step-based scheduler with a decay gamma of 0.1 for all model training. All disease classification and reconstruction models are trained for 50 epochs, and the severity classification model is fine-tuned for 20 epochs. For the policy model, we train it for 30 epochs. Our experimental setup uses the PyTorch framework, and all computations are performed on an NVIDIA A100 Tensor Core GPU.

V. EXPERIMENTAL RESULTS AND ANALYSIS

We divide this section into several parts, each addressing key questions/hypotheses. First, we aim to show that our

approach maintains diagnostic performance when compared to other non-sequential and single objective policies. We then proceed to address our main hypothesis that adopting sequential decisions leads to k -space savings. Finally, we show that the natural ordering of the objectives results in even more savings.

A. Comparison to Non-sequential and Single Objective Policies

In this section, we first answer a critical question: *Will our method compromise performance when enforcing multiple objectives in a single scan?* We compare the diagnostic accuracy of our sequential diagnosis method with baselines and benchmarks designed for a single binary diagnosis task, namely the *Undersampled*, *Policy Recon*, and *Policy Classifier*, at various sample rates for inferring the conditions of ACL Sprain and Cartilage Thickness Loss. *Undersampled* randomly samples k -space lines progressively. *Policy Recon*, *Policy Classifier*, and *Weighted Policy* start with a randomly initialized mask at a sample rate of 5% and perform sampling decision-making respectively using their policies (see Section IV-B). We also include *Fully sampled* as a diagnostic oracle, which does not have a sampling budget. The results are shown in Table III and Table IV.

Our *Weighted Policy*, consistently demonstrates strong performance in all metrics across different sampling rates and both tasks (ACL Sprain and Thickness Loss). Focusing first on Table III, we observe that: (i) *Weighted Policy* matches the performance of *Fully Sampled*, showing that careful selection of k -space lines avoids taking redundant and irrelevant information. (ii) The advantage of policy-based optimization in our method is clearly demonstrated as we can match the performance of *Fully Sampled* with roughly 10% k -space data across all subtasks. (iii) As expected, *Policy Recon*, which optimizes reconstruction performance, underperforms our approach which optimizes for each task at hand. (iv) More importantly, our *Weighted Policy*, which jointly optimizes disease detection and severity quantification, outperforms the *Policy Classifier* in most cases even when used for a single subtask with fewer samples. In fact, with 10% sampling in disease detection (84.20% vs. 81.32%) and 20% k -space sampling for severity quantification (74.10% vs. 74.08%), this finding is extremely important, as it answers the initially posed question. It demonstrates that a policy optimized for multiple objectives does not compromise diagnostic performance compared to policies optimized for a single objective.

Similar observations hold for Cartilage Thickness Loss in Table IV, evidently illustrating the applicability of our methods in two settings and hence the strength of our findings.

B. k -space Savings

We now proceed to answer our main hypothesis: *Joint optimization of a policy for two objectives ultimately leads to sampling efficiency and savings.*

In Figure 4, we illustrate the diagnostic performance of policies that progressively make decisions on which line to acquire, line-by-line, and visualize their sampling trajectories.

TABLE III

AVERAGE BALANCED ACCURACY (%) AND AREA UNDER CURVE (%) RESULTS AND THE STANDARD DEVIATIONS OF DIFFERENT DIAGNOSTIC POLICIES ACROSS VARYING SAMPLING RATES FOR ACL SPRAIN DIAGNOSIS. DASHES (—) INDICATE SCENARIOS WHERE THE METHOD IS NOT APPLICABLE. BOLD NUMBERS DENOTE THE BEST PERFORMANCE

Diagnosis Task		Disease					Severity Degree					Sequential Diagnosis					
		84.27 _{0.0}	—	—	—	—	69.90 _{1.5}	—	—	—	—	65.94 _{0.1}	—	—	—	—	
Fully Sampled (Oracle)		84.27 _{0.0}	—	—	—	—	69.90 _{1.5}	—	—	—	—	65.94 _{0.1}	—	—	—	—	
Sampling Rate	5%	10%	15%	20%	30%	5%	10%	15%	20%	30%	5%	10%	15%	20%	30%	5%	
Undersampled	72.90 _{2.9}	75.68 _{2.5}	76.14 _{1.9}	76.58 _{1.8}	79.64 _{0.8}	60.62 _{1.7}	61.20 _{3.0}	62.90 _{3.1}	64.58 _{4.0}	68.42 _{2.5}	—	—	—	—	—	—	
Policy Classifier [4]	72.90 _{2.9}	81.32 _{1.7}	81.78 _{1.4}	81.84 _{0.7}	82.94 _{0.8}	60.62 _{1.7}	71.94 _{2.7}	74.08 _{2.3}	74.64 _{1.9}	78.58 _{2.6}	—	—	—	—	—	—	
Policy Recon [18]	62.54 _{0.1}	69.60 _{0.4}	78.60 _{0.4}	79.14 _{0.2}	81.92 _{0.5}	37.70 _{0.0}	30.32 _{1.9}	43.08 _{2.7}	49.14 _{0.1}	54.64 _{2.1}	41.90 _{0.0}	39.68 _{0.7}	52.44 _{1.7}	55.22 _{0.1}	60.40 _{1.1}	60.40 _{1.1}	
Weighted Policy (Ours)	73.26 _{2.8}	84.20 _{1.3}	84.76 _{1.0}	84.34 _{0.7}	83.54 _{0.4}	58.94 _{4.1}	76.86 _{2.8}	74.10 _{3.1}	73.88 _{1.9}	75.36 _{2.8}	53.58 _{3.1}	73.42 _{2.0}	72.36 _{1.9}	71.72 _{1.7}	71.68 _{1.6}	71.68 _{1.6}	
Diagnosis Task		Disease					Severity Degree					Sequential Diagnosis					
		90.23 _{0.0}	—	—	—	—	71.03 _{1.2}	—	—	—	—	80.76 _{0.1}	—	—	—	—	
Fully Sampled (Oracle)		90.23 _{0.0}	—	—	—	—	71.03 _{1.2}	—	—	—	—	80.76 _{0.1}	—	—	—	—	
Sampling Rate	5%	10%	15%	20%	30%	5%	10%	15%	20%	30%	5%	10%	15%	20%	30%	5%	
Undersampled	84.10 _{1.8}	85.58 _{1.3}	86.50 _{1.2}	87.28 _{1.3}	88.40 _{0.7}	69.20 _{4.6}	70.34 _{5.5}	73.38 _{4.5}	75.36 _{4.2}	79.70 _{4.7}	—	—	—	—	—	—	
Policy Classifier [4]	84.10 _{1.8}	88.72 _{0.5}	88.64 _{0.5}	88.54 _{0.4}	88.98 _{0.4}	69.20 _{4.6}	83.78 _{1.7}	84.80 _{1.3}	85.10 _{1.4}	87.16 _{1.5}	—	—	—	—	—	—	
Policy Recon [18]	78.16 _{0.1}	84.02 _{0.1}	87.98 _{0.0}	88.44 _{0.1}	89.30 _{0.1}	35.80 _{0.0}	25.40 _{0.5}	42.10 _{0.8}	46.66 _{0.4}	57.86 _{0.9}	56.98 _{0.0}	54.72 _{0.3}	65.02 _{0.4}	67.56 _{0.2}	73.58 _{0.4}	73.58 _{0.4}	
Weighted Policy (Ours)	83.24 _{1.5}	89.32 _{0.4}	89.54 _{0.2}	89.50 _{0.1}	89.36 _{0.3}	67.22 _{5.5}	88.14 _{1.2}	86.76 _{1.4}	86.08 _{1.0}	87.44 _{1.1}	75.22 _{3.0}	88.72 _{0.6}	88.14 _{0.8}	87.78 _{0.5}	88.40 _{0.7}	88.40 _{0.7}	
Diagnosis Task		Disease					Severity Degree					Sequential Diagnosis					
		90.23 _{0.0}	—	—	—	—	71.03 _{1.2}	—	—	—	—	80.76 _{0.1}	—	—	—	—	
Fully Sampled (Oracle)		90.23 _{0.0}	—	—	—	—	71.03 _{1.2}	—	—	—	—	80.76 _{0.1}	—	—	—	—	
Sampling Rate	5%	10%	15%	20%	30%	5%	10%	15%	20%	30%	5%	10%	15%	20%	30%	5%	
Undersampled	84.10 _{1.8}	85.58 _{1.3}	86.50 _{1.2}	87.28 _{1.3}	88.40 _{0.7}	69.20 _{4.6}	70.34 _{5.5}	73.38 _{4.5}	75.36 _{4.2}	79.70 _{4.7}	—	—	—	—	—	—	
Policy Classifier [4]	84.10 _{1.8}	88.72 _{0.5}	88.64 _{0.5}	88.54 _{0.4}	88.98 _{0.4}	69.20 _{4.6}	83.78 _{1.7}	84.80 _{1.3}	85.10 _{1.4}	87.16 _{1.5}	—	—	—	—	—	—	
Policy Recon [18]	78.16 _{0.1}	84.02 _{0.1}	87.98 _{0.0}	88.44 _{0.1}	89.30 _{0.1}	35.80 _{0.0}	25.40 _{0.5}	42.10 _{0.8}	46.66 _{0.4}	57.86 _{0.9}	56.98 _{0.0}	54.72 _{0.3}	65.02 _{0.4}	67.56 _{0.2}	73.58 _{0.4}	73.58 _{0.4}	
Weighted Policy (Ours)	83.24 _{1.5}	89.32 _{0.4}	89.54 _{0.2}	89.50 _{0.1}	89.36 _{0.3}	67.22 _{5.5}	88.14 _{1.2}	86.76 _{1.4}	86.08 _{1.0}	87.44 _{1.1}	75.22 _{3.0}	88.72 _{0.6}	88.14 _{0.8}	87.78 _{0.5}	88.40 _{0.7}	88.40 _{0.7}	

TABLE IV
SAME AS IN TABLE III BUT FOR CARTILAGE THICKNESS LOSS

Diagnosis Task		Disease					Severity Degree					Sequential Diagnosis					
		75.05 _{0.1}	—	—	—	—	60.90 _{2.7}	—	—	—	—	54.84 _{0.0}	—	—	—	—	
Fully Sampled (Oracle)		75.05 _{0.1}	—	—	—	—	60.90 _{2.7}	—	—	—	—	54.84 _{0.0}	—	—	—	—	
Sampling Rate	5%	10%	15%	20%	30%	5%	10%	15%	20%	30%	5%	10%	15%	20%	30%	5%	
Undersampled	71.12 _{3.0}	73.22 _{1.2}	74.32 _{0.9}	74.62 _{1.4}	75.22 _{1.4}	54.90 _{2.3}	59.42 _{3.0}	59.02 _{3.0}	60.32 _{3.3}	61.38 _{2.8}	—	—	—	—	—	—	
Policy Classifier [4]	71.12 _{3.0}	73.72 _{2.5}	75.14 _{1.1}	75.30 _{1.3}	75.98 _{1.2}	54.90 _{2.3}	58.58 _{4.0}	60.30 _{1.4}	63.10 _{3.9}	63.84 _{5.0}	—	—	—	—	—	—	
Policy Recon [18]	64.34 _{0.1}	65.86 _{0.9}	72.18 _{0.3}	71.20 _{0.3}	75.92 _{0.4}	56.58 _{0.0}	56.68 _{1.0}	54.50 _{0.9}	55.18 _{0.9}	56.60 _{0.9}	45.22 _{0.0}	44.72 _{1.3}	50.18 _{0.7}	50.16 _{0.1}	54.46 _{0.7}	54.46 _{0.7}	
Weighted Policy (Ours)	72.76 _{1.5}	72.96 _{1.0}	74.02 _{0.9}	73.86 _{1.1}	73.84 _{1.5}	58.92 _{5.7}	60.62 _{3.9}	58.98 _{2.8}	60.88 _{2.5}	62.32 _{3.0}	54.40 _{2.8}	54.88 _{2.1}	53.90 _{2.2}	54.80 _{0.9}	55.48 _{0.6}	55.48 _{0.6}	
Diagnosis Task		Disease					Severity Degree					Sequential Diagnosis					
		88.23 _{0.0}	—	—	—	—	73.58 _{4.2}	—	—	—	—	80.88 _{0.5}	—	—	—	—	
Fully Sampled (Oracle)		88.23 _{0.0}	—	—	—	—	73.58 _{4.2}	—	—	—	—	80.88 _{0.5}	—	—	—	—	
Sampling Rate	5%	10%	15%	20%	30%	5%	10%	15%	20%	30%	5%	10%	15%	20%	30%	5%	
Undersampled	84.58 _{1.0}	86.02 _{0.7}	87.38 _{0.3}	87.86 _{0.7}	88.08 _{0.6}	61.90 _{5.0}	66.40 _{7.4}	68.76 _{5.3}	71.80 _{5.4}	76.82 _{4.5}	—	—	—	—	—	—	
Policy Classifier [4]	84.58 _{1.0}	86.74 _{0.4}	87.32 _{0.4}	87.82 _{0.4}	87.96 _{0.4}	61.90 _{5.0}	81.12 _{2.0}	83.10 _{1.6}	83.24 _{1.3}	85.26 _{1.4}	—	—	—	—	—	—	
Policy Recon [18]	83.72 _{0.0}	85.30 _{0.1}	86.18 _{0.1}	86.42 _{0.0}	87.38 _{0.0}	71.44 _{1.1}	68.32 _{0.9}	71.30 _{0.6}	70.52 _{0.6}	75.00 _{0.9}	77.58 _{0.0}	76.84 _{0.4}	78.74 _{0.3}	78.48 _{0.3}	81.22 _{0.4}	81.22 _{0.4}	
Weighted Policy (Ours)	85.24 _{0.8}	87.34 _{0.3}	89.06 _{0.4}	89.88 _{0.3}	89.02 _{0.3}	65.70 _{6.1}	75.04 _{1.2}	80.94 _{1.6}	83.60 _{1.0}	85.58 _{1.5}	75.44 _{3.2}	81.20 _{0.6}	84.98 _{0.8}	86.28 _{0.6}	87.26 _{0.8}	87.26 _{0.8}	

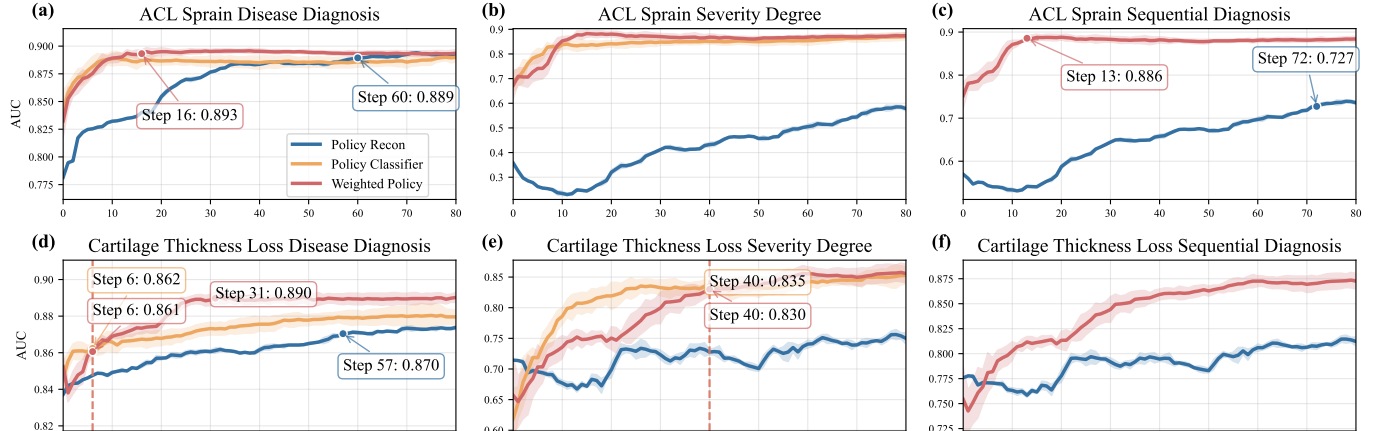


Fig. 4. Performance comparison of our proposed *Weighted Policy* and two single-task oriented policies. The horizontal axis indicates the cumulative lines acquired when sampling. The 80-step active sampling procedure starts from 16 randomly sampled *k*-space lines.

We present the performance of our method and compare with *Policy Recon* and *Policy Classifier* to showcase the difference between sampling patterns of single-task methods versus ours.

We find that the performance curve plateaus during the sampling process, indicating that the policies might have collected the majority of diagnostically significant *k*-space lines that contribute to diagnostic performance enhancement.

For disease detection, as shown in Figure 4 (a) and (d), compared to *Policy Recon* which optimizes sampling trajectories for reconstruction, our method plateaus earlier at step 16 for ACL Sprain, whereas *Policy Recon* plateaus much later (at step 60 for ACL Sprain leading to considerable *k*-space savings. The

advantage of a diagnosis-oriented policy is further highlighted in severity quantification (Figure 4 (b)), where our method successfully identifies *k*-space lines that can significantly improve inference. In contrast, although it can achieve continuous improvements in reconstruction performance, *Policy Recon* struggles to effectively locate diagnostically relevant *k*-space lines and produce comparable outcomes in both severity and sequential diagnosis classification. Consequently, when evaluating sequential diagnosis in ACL Sprain (Figure 4 (c)), our method reaches a plateau at step 13 with a high balanced accuracy of 0.886, while *Policy Recon* arrives at step 72 with a balanced accuracy of 0.727. Similar observations hold for

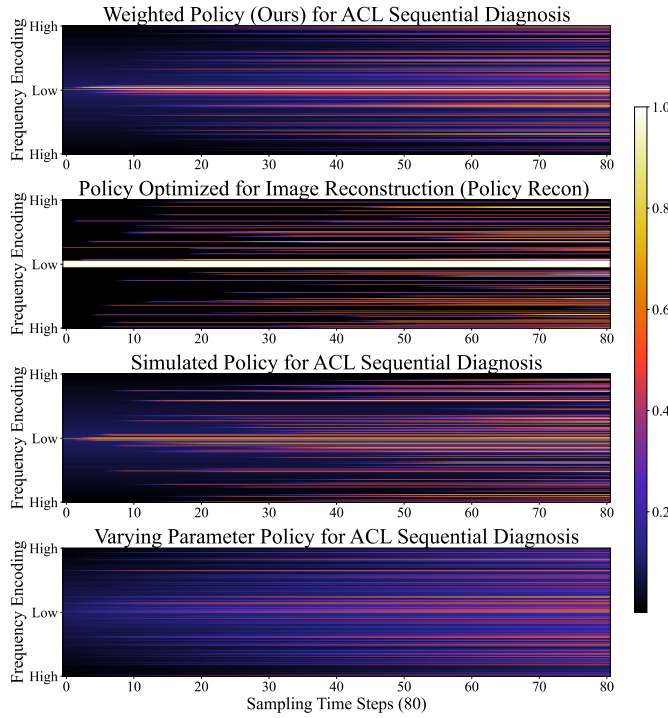


Fig. 5. Average k -space sampling behaviors across all subjects of our proposed *Weighted Policy* and benchmarks. A High value in the plot represents a high probability to be sampled. The horizontal axis indicates the cumulative lines acquired when sampling.

Cartilage Thickness Loss (Figure 4 (d) to (f)).

In Figure 4, compared to the policies of *Policy Classifier* that optimize sampling trajectories independently for separate tasks (disease detection or severity quantification), our method provides competitive results and achieves considerable acquisition savings. For ACL Sprain, our policy quickly matches the performance of *Policy Classifiers*, and exceeds them afterward. Similarly, as shown in plots (d) and (e), *Weighted Policy* samples 6 lines in disease detection and 40 lines in severity quantification for Cartilage Thickness Loss to achieve the performance of the corresponding *Policy Classifier*. Notably, our policy achieves this sequentially whereas the other policies require different sessions for two tasks. Hence, our method can significantly reduce the quantity of necessary k -space lines and thereby shorten the acquisition time.

Next, we want to compare the sampling behaviors of different policies averaged across the subject population. As shown in Figure 5, referring to the top two plots, there are evident differences between the trajectories of *Policy Recon* and *Weighted Policy*. *Policy Recon* tends to consistently sample low-frequency central k -space lines, whereas our method shows a broader diversity (across the frequency spectrum), illustrating its adaptation at the patient level.

C. Sequential Diagnosis in One Scanning Session

We base our work on a key question: *Is it necessary to adopt a sequential process, detecting disease first and then assessing severity?* This question is crucial because our proposed sequential diagnosis workflow employs the lexicographic ordering in step-wise weighting module, attempting

to mirror the clinical workflow of radiologists. To address this key question, we train two policies with different ways to optimize for multiple objectives in parallel and independently. The first, termed *Simulated Policy*, uses the same architecture as ours but employs a single-objective RL algorithm rewarded by the performance of a three-way diagnosis (no finding, low, or high severity) without specifying the lexicographic ordering among diagnostic objectives. The second, the *Varying Parameter Policy*, is instead a MORL-based method, which uses separate policy networks to optimize detection and quantification in parallel as independent objectives, and the final sampling policy is the average of the result of the two policy networks.

Referring to Figure 6 and first focusing on comparisons with the *Simulated Policy*, we see that the *Simulated Policy* plateaus earlier at a lower performance compared to our method. This is because the *Simulated Policy* is rewarded based on overall sequential diagnosis improvements, forcing the policy to find k -space lines that contribute to a three-way objective, therefore lacking reward information for each independent objective. Our method explicitly calculates the separate rewards of the two objectives, which simplifies the sequential diagnosis task and reduces the complexity of the sampling strategy optimization.

We compare with *Varying Parameter Policy*, a MORL-based trained policy, whose key differences are: (i) it employs individual policies to process rewards from the independent objectives in parallel; and most importantly, (ii) it does not utilize the lexicographic ordering between objectives. Thus, we expect to observe worse performance for this ‘simpler’ policy. Looking again at Figure 6, and now comparing the ‘grey’ (*Varying Parameter Policy*) and ‘red’ (*Weighted Policy*) lines, our method outperforms the other policy and plateaus earlier at a higher accuracy level, particularly in the overall sequential diagnosis (Figure 6 (c) and (f)), hence achieving k -space sampling savings and in turn less scanning time. This highlights the benefits of lexicographic ordering in multi-objective optimization and step-wise weighting. Our policy thus learns the inherent shared diagnostic features between disease detection and severity quantification, and is encouraged to seek mutually beneficial lines during sampling. Consequently, in Figure 6 Cartilage Thickness Loss, after sampling what is needed to decide in the presence of disease (shown as plateauing at step 31 subplot (d)), the optimization prioritizes sampling of k -space lines that contribute to severity as observed by an increase in performance in the subplot (e) without compromising disease diagnosis performance (the plateau).

We can observe such transitions also at the level of sampling trajectories in Figure 5 as well. Looking at the bottom two plots and comparing them with the topmost, until sampling step 16, our proposed policy samples more low-frequency lines (containing structural information) that can contribute to both objectives and patient-level disease-related information (shown as purple in the plot). Then, the policy smoothly shifts to sampling diagnostic features located in high-frequency zone, which may contribute to severity quantification for ACL Sprain. While *Varying Parameter Policy* tends to find patient-level features from the start, it can miss the mutual diagnosti-

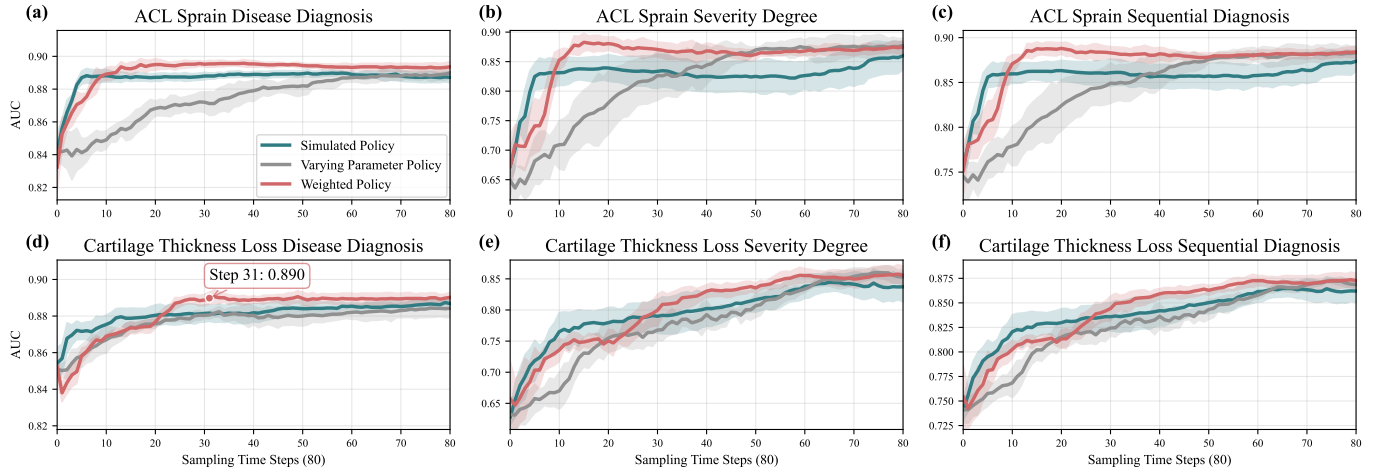


Fig. 6. Performance comparison of our proposed *Weighted Policy* and two multi-task oriented policies. The horizontal axis indicates the cumulative lines acquired when sampling. The 80-step active sampling procedure starts from 16 randomly sampled k -space lines.

cially significant lines between disease detection and severity quantification. The probability trajectories of the *Simulated Policy* show several frequency locations with high sampling probability, illustrating a tendency to generate similar sampling trajectories for all subjects, thereby lacking exploration of patient-level diagnostic information.

VI. DISCUSSIONS AND CONCLUSION

A. Clinical Relevance

Our framework enables the efficient acquisition of diagnostically relevant k -space data while sequentially performing disease detection and severity quantification in a single scanning session. This approach enables comprehensive assessment during the scanning process, potentially eliminating the need for follow-up examinations. The sequential diagnosis paradigm completes multi-objective diagnostic tasks within a single scanning session without requiring full k -space acquisition, thereby significantly reducing MRI acquisition time.

The acquisition acceleration of the proposed pipeline via patient-level active sampling could substantially enhance the clinical utility of low-field MRI, making them more viable for PoC applications [1]. We envision practical implementations in preliminary screening scenarios where rapid assessments are crucial to guide resource allocation decisions [42], which is particularly valuable in settings with limited healthcare infrastructure or in emergency medicine contexts [43] where time-critical diagnostic information is essential.

B. Limitations

Our method has been implemented as a proof-of-concept on the fastMRI knee dataset, focusing on specific pathologies where data are publicly available. Future work could explore other applications such as stroke [44] or acute brain trauma diagnosis [43], where rapid assessment from limited data is crucial. Although such datasets are not publicly available, we hope our open-source code will encourage researchers with access to evaluate our method in these critical settings.

Our current implementation relies on pre-trained classifiers, which may propagate inherent biases and exhibit vulnerability to domain shifts when applied to new data distributions [45]. An important direction for future research is to explore end-to-end joint optimization of classification and policy networks, potentially through meta-learning approaches that could adapt to new diagnostic tasks with minimal fine-tuning.

C. Conclusion

We propose a novel MORL framework for sequential diagnostic assessment directly from undersampled k -space data. By structuring clinical diagnosis as a sequential decision process with lexicographic ordering, our method achieves diagnostic performance on par with fully sampled references while significantly reducing acquisition time. Empirical results on two datasets show that our diagnosis-oriented sampling strategy surpasses reconstruction-based methods in both diagnostic accuracy and efficiency. Compared to single-objective diagnostic samplers, our approach achieves substantial k -space savings within a single scan without compromising performance. Our step-wise weighting mechanism effectively prioritizes disease detection early in the acquisition before transitioning to severity assessment, thereby aligning with clinical workflows. Furthermore, the convergence of sampling trajectories across tasks supports the existence of shared informative k -space regions, enabling efficient, comprehensive assessment in a single session. This work advances direct k -space inference, paving the way for clinically viable, PoC MRI diagnostics with reduced acquisition demands.

REFERENCES

- [1] S. Geethanath and J. T. Vaughan Jr, “Accessible magnetic resonance imaging: a review,” *Journal of Magnetic Resonance Imaging*, vol. 49, no. 7, pp. e65–e77, 2019.
- [2] Y. Anzai and L. Moy, “Point-of-care low-field-strength mri is moving beyond the hype,” pp. 672–673, 2022.
- [3] M. Hori, A. Hagiwara, M. Goto, A. Wada, and S. Aoki, “Low-field magnetic resonance imaging: its history and renaissance,” *Investigative radiology*, vol. 56, no. 11, pp. 669–679, 2021.

[4] Y. Du, R. Dharmakumar, and S. A. Tsaftaris, "The MRI scanner as a diagnostic: image-less active sampling," in *International Conference on Medical Image Computing and Computer-Assisted Intervention*. Springer, 2024, pp. 467–476.

[5] D. J. Lin, P. M. Johnson, F. Knoll, and Y. W. Lui, "Artificial intelligence for mr image reconstruction: an overview for clinicians," *Journal of Magnetic Resonance Imaging*, vol. 53, no. 4, pp. 1015–1028, 2021.

[6] C. D. Bahadir, A. Q. Wang, A. V. Dalca, and M. R. Sabuncu, "Deep-learning-based optimization of the under-sampling pattern in mri," *IEEE Transactions on Computational Imaging*, vol. 6, pp. 1139–1152, 2020.

[7] Z. Zhang, A. Romero, M. J. Muckley, P. Vincent, L. Yang, and M. Drozdal, "Reducing uncertainty in undersampled mri reconstruction with active acquisition," in *Proceedings of the IEEE/CVF conference on computer vision and pattern recognition*, 2019, pp. 2049–2058.

[8] R. Singhal, M. Sudarshan, A. Mahishi, S. Kaushik, L. Ginocchio, A. Tong, H. Chandarana, D. K. Sodickson, R. Ranganath, and S. Chopra, "On the feasibility of machine learning augmented magnetic resonance for point-of-care identification of disease," *arXiv preprint arXiv:2301.11962*, 2023.

[9] C.-Y. Yen, R. Singhal, U. Sharma, R. Ranganath, S. Chopra, and L. Pinto, "Adaptive sampling of k-space in magnetic resonance for rapid pathology prediction," *arXiv preprint arXiv:2406.04318*, 2024.

[10] G. Zeng, Y. Guo, J. Zhan, Z. Wang, Z. Lai, X. Du, X. Qu, and D. Guo, "A review on deep learning mri reconstruction without fully sampled k-space," *BMC Medical Imaging*, vol. 21, no. 1, p. 195, 2021.

[11] G. Yiayiannis, C. I. Sánchez, J.-J. Sonke, and J. Teuwen, "On retrospective k-space subsampling schemes for deep mri reconstruction," *Magnetic Resonance Imaging*, vol. 107, pp. 33–46, 2024.

[12] J. Wang, Q. Yang, Q. Yang, L. Xu, C. Cai, and S. Cai, "Joint optimization of cartesian sampling patterns and reconstruction for single-contrast and multi-contrast fast magnetic resonance imaging," *Computer Methods and Programs in Biomedicine*, vol. 226, p. 107150, 2022.

[13] J. Zhang, H. Zhang, A. Wang, Q. Zhang, M. Sabuncu, P. Spincemaille, T. D. Nguyen, and Y. Wang, "Extending loupe for k-space undersampling pattern optimization in multi-coil mri," in *Machine Learning for Medical Image Reconstruction: Third International Workshop, MLMIR 2020, Held in Conjunction with MICCAI 2020, Lima, Peru, October 8, 2020, Proceedings 3*. Springer, 2020, pp. 91–101.

[14] G. Wang, T. Luo, J.-F. Nielsen, D. C. Noll, and J. A. Fessler, "B-spline parameterized joint optimization of reconstruction and k-space trajectories (bjork) for accelerated 2d mri," *IEEE Transactions on Medical Imaging*, vol. 41, no. 9, pp. 2318–2330, 2022.

[15] G. Wang and J. A. Fessler, "Efficient approximation of jacobian matrices involving a non-uniform fast fourier transform (nufft)," *IEEE transactions on computational imaging*, vol. 9, pp. 43–54, 2023.

[16] S. Ravula, B. Levac, A. Jalal, J. I. Tamir, and A. G. Dimakis, "Optimizing sampling patterns for compressed sensing mri with diffusion generative models," *arXiv preprint arXiv:2306.03284*, 2023.

[17] K. Xuan, S. Sun, Z. Xue, Q. Wang, and S. Liao, "Learning mri k-space subsampling pattern using progressive weight pruning," in *Medical Image Computing and Computer Assisted Intervention–MICCAI 2020: 23rd International Conference, Lima, Peru, October 4–8, 2020, Proceedings, Part II 23*. Springer, 2020, pp. 178–187.

[18] T. Bakker, H. van Hoof, and M. Welling, "Experimental design for MRI by greedy policy search," *Advances in Neural Information Processing Systems*, vol. 33, pp. 18954–18966, 2020.

[19] L. Pineda, S. Basu, A. Romero, R. Calandra, and M. Drozdal, "Active mr k-space sampling with reinforcement learning," in *International Conference on Medical Image Computing and Computer-Assisted Intervention*. Springer, 2020, pp. 23–33.

[20] J. Schlemper, O. Oktay, W. Bai, D. C. Castro, J. Duan, C. Qin, J. V. Hajnal, and D. Rueckert, "Cardiac mr segmentation from undersampled k-space using deep latent representation learning," in *Medical Image Computing and Computer Assisted Intervention–MICCAI 2018: 21st International Conference, Granada, Spain, September 16–20, 2018, Proceedings, Part I*. Springer, 2018, pp. 259–267.

[21] Y. Zhao, X. Wang, T. Che, G. Bao, and S. Li, "Multi-task deep learning for medical image computing and analysis: A review," *Computers in Biology and Medicine*, vol. 153, p. 106496, 2023.

[22] H. Huang, G. Yang, W. Zhang, X. Xu, W. Yang, W. Jiang, and X. Lai, "A deep multi-task learning framework for brain tumor segmentation," *Frontiers in oncology*, vol. 11, p. 690244, 2021.

[23] C. Yu, J. Liu, S. Nemat, and G. Yin, "Reinforcement learning in healthcare: A survey," *ACM Computing Surveys (CSUR)*, vol. 55, no. 1, pp. 1–36, 2021.

[24] W. Han, C. Kim, D. Ju, Y. Shim, and S. J. Hwang, "Advancing text-driven chest x-ray generation with policy-based reinforcement learning," in *International Conference on Medical Image Computing and Computer-Assisted Intervention*. Springer, 2024, pp. 56–66.

[25] A. Vlontzos, A. Alansary, K. Kamnitsas, D. Rueckert, and B. Kainz, "Multiple landmark detection using multi-agent reinforcement learning," in *Medical Image Computing and Computer Assisted Intervention–MICCAI 2019: 22nd International Conference, Shenzhen, China, October 13–17, 2019, Proceedings, Part IV 22*. Springer, 2019, pp. 262–270.

[26] D. Zhang, B. Chen, and S. Li, "Sequential conditional reinforcement learning for simultaneous vertebral body detection and segmentation with modeling the spine anatomy," *Medical image analysis*, vol. 67, p. 101861, 2021.

[27] S. N. Khatami and C. Gopalappa, "A reinforcement learning model to inform optimal decision paths for hiv elimination," *Mathematical biosciences and engineering: MBE*, vol. 18, no. 6, p. 7666, 2021.

[28] X. Liao, W. Li, Q. Xu, X. Wang, B. Jin, X. Zhang, Y. Wang, and Y. Zhang, "Iteratively-refined interactive 3d medical image segmentation with multi-agent reinforcement learning," in *Proceedings of the IEEE/CVF conference on computer vision and pattern recognition*, 2020, pp. 9394–9402.

[29] E. J. Sondik, *The optimal control of partially observable Markov processes*. Stanford University, 1971.

[30] W. Kool, H. van Hoof, and M. Welling, "Buy 4 REINFORCE samples, get a baseline for free!" 2019. [Online]. Available: <https://openreview.net/forum?id=r1lgTGL5DE>

[31] R. C. of Radiologists, "Standards for interpretation and reporting of imaging investigations," 2018.

[32] J. Skalse, L. Hammond, C. Griffin, and A. Abate, "Lexicographic multi-objective reinforcement learning," *arXiv preprint arXiv:2212.13769*, 2022.

[33] E. Maeland, "On the comparison of interpolation methods," *IEEE Transactions on Medical Imaging*, vol. 7, no. 3, pp. 213–217, 1988.

[34] J. Zbontar, F. Knoll, A. Sriram, T. Murrell, Z. Huang, M. J. Muckley, A. Defazio, R. Stern, P. Johnson, M. Bruno *et al.*, "fastmri: An open dataset and benchmarks for accelerated mri," *arXiv preprint arXiv:1811.08839*, 2018.

[35] R. Zhao, B. Yaman, Y. Zhang, R. Stewart, A. Dixon, F. Knoll, Z. Huang, Y. W. Lui, M. S. Hansen, and M. P. Lungren, "fastmri+, clinical pathology annotations for knee and brain fully sampled magnetic resonance imaging data," *Scientific Data*, vol. 9, no. 1, p. 152, 2022.

[36] O. Ronneberger, P. Fischer, and T. Brox, "U-net: Convolutional networks for biomedical image segmentation," in *Medical image computing and computer-assisted intervention–MICCAI 2015: 18th international conference, Munich, Germany, October 5–9, 2015, proceedings, part III 18*. Springer, 2015, pp. 234–241.

[37] Z. Wang, A. C. Bovik, H. R. Sheikh, and E. P. Simoncelli, "Image quality assessment: from error visibility to structural similarity," *IEEE transactions on image processing*, vol. 13, no. 4, pp. 600–612, 2004.

[38] C. Liu, X. Xu, and D. Hu, "Multiobjective reinforcement learning: A comprehensive overview," *IEEE Transactions on Systems, Man, and Cybernetics: Systems*, vol. 45, no. 3, pp. 385–398, 2014.

[39] K. He, X. Zhang, S. Ren, and J. Sun, "Deep residual learning for image recognition," in *Proceedings of the IEEE conference on computer vision and pattern recognition*, 2016, pp. 770–778.

[40] A. Mao, M. Mohri, and Y. Zhong, "Cross-entropy loss functions: Theoretical analysis and applications," in *Proceedings of the 40th International Conference on Machine Learning*, ser. Proceedings of Machine Learning Research, vol. 202. PMLR, 2023, pp. 23 803–23 828.

[41] D. P. Kingma and J. Ba, "Adam: A method for stochastic optimization," *arXiv preprint arXiv:1412.6980*, 2014.

[42] A. P. Brady, J. A. Bello, L. E. Derchi, M. Fuchsäger, S. Goergen, G. P. Krestin, E. J. Lee, D. C. Levin, J. Pressacco, V. M. Rao *et al.*, "Radiology in the era of value-based healthcare: a multi-society expert statement from the acr, car, esr, is3r, ranzcr, and rsna," *Canadian Association of Radiologists Journal*, vol. 72, no. 2, pp. 208–214, 2021.

[43] M. H. Mazurek, B. A. Cahn, M. M. Yuen, A. M. Prabhat, I. R. Chavva, J. T. Shah, A. L. Crawford, E. B. Welch, J. Rothberg, L. Sacolick *et al.*, "Portable, bedside, low-field magnetic resonance imaging for evaluation of intracerebral hemorrhage," *Nature communications*, vol. 12, no. 1, p. 5119, 2021.

[44] K. C. Ho, F. Scalzo, K. V. Sarma, W. Speier, S. El-Saden, and C. Arnold, "Predicting ischemic stroke tissue fate using a deep convolutional neural network on source magnetic resonance perfusion images," *Journal of Medical Imaging*, vol. 6, no. 2, pp. 026 001–026 001, 2019.

[45] C. Wachinger, A. Rieckmann, S. Pöhlsterl, A. D. N. Initiative *et al.*, "Detect and correct bias in multi-site neuroimaging datasets," *Medical Image Analysis*, vol. 67, p. 101879, 2021.